NASA Technical Memorandum 102418

Thermal Modelling of Various Thermal Barrier Coatings in a High Heat Flux Rocket Engine

James A. Nesbitt
Lewis Research Center
Cleveland, Ohio

December 1989

THERMAL MODELLING OF VARIOUS THERMAL BARRIER COATINGS IN A HIGH HEAT FLUX ROCKET ENGINE

James A. Nesbitt
National Aeronautics and Space Administration
Lewis Research Center
Cleveland, Ohio 44135

air plasma sprayed
thermal barrier coatings
low pressure plasma sprayed

SUMMARY

Traditional APS ZrO_2-Y_2O_3 TBC's and APS and LPPS ZrO_2-Y_2O_3/Ni-Cr-Al-Y cermet coatings were tested in a H_2/O_2 rocket engine ~~located at the NASA Lewis Research Center~~. The traditional ZrO_2-Y_2O_3 ~~thermal~~ barrier coatings (TBC's) showed considerable metal temperature reductions during testing in the hydrogen-rich environment. A thermal model was developed to predict the thermal response of the tubes with the various coatings. Good agreement was observed between predicted temperatures and measured temperatures at the inner wall of the tube and in the metal near the coating/metal interface.

micron

The thermal model was also used to examine the effect of the differences in the reported values of the thermal conductivity of plasma sprayed ZrO_2-Y_2O_3 ceramic coatings, the effect of a 100 µm (0.004 in.) thick metallic bond coat, the effect of tangential heat transfer around the tube, and the effect of radiation from the surface of the ceramic coating. It was shown that for the short duration testing in the rocket engine, the most important of these considerations was the effect of the uncertainty in the thermal conductivity of traditional APS ZrO_2-Y_2O_3 TBC's which can amount to significantly different temperatures (>100 °C) predicted in the tube. The thermal model was also used to predict the thermal response of a coated rod in order to quantify the difference in the metal temperatures between the two substrate geometries and to explain the previously-observed increased life of coatings on rods over that on tubes.

[illegible] than

A thermal model was also developed to predict heat transfer to the leading edge of HPFTP blades during start-up of the space shuttle main engines. The ability of various TBC's to reduce metal temperatures during the two thermal excursions occurring on start-up was predicted. Temperature reductions of 150 to 470 °C were predicted for 165 µm (0.0065 in.) coatings for the greater of the two thermal excursions.

micron

high pressure fuel turbopump

INTRODUCTION

The blades in the high-pressure fuel turbopump (HPFTP) on the space shuttle main engines (SSME) undergo extreme thermal transients on start-up of the engines. The thermal shock to these blades is believed to contribute to crack formation and/or crack propagation which has led to the early replacement of the blades far short of the desired design life. During early development work on the SSME, thermal barrier coatings (TBC's) were examined as a means of reducing the thermal shock to these blades. However, spallation of the ceramic top layer during test firings resulted in dropping from consideration the use of ceramic coatings. Currently, only a metallic coating, providing minimal thermal protection, is applied to HPFTP blades.

E-5184

Recent advances in TBC technology prompted a re-examination of the use of thermal barrier coatings for HPFTP blades (refs. 1 and 2). A hydrogen/oxygen rocket engine was developed at NASA Lewis Research Center to test the durability of various TBC's in a high heat flux environment. Numerous thermal barrier coatings on tube and rod substrates were tested (ref. 2). This study found that, in general, coatings were more durable on rod substrates than on tubes. This increased durability can be attributed to lower coating and substrate temperatures due to the greater thermal mass of the rod, although temperature measurements on rod substrates were not performed to quantify this temperature reduction.

The purpose of the present work was to examine the thermal transport and evaluate the thermal protection of several different TBC's tested in the rocket engine at NASA Lewis. These coatings included traditional TBC's with a ZrO_2-Y_2O_3 top coat and Ni-Cr-Al-Y bond coat, as well as two cermet coatings consisting of different amounts of ZrO_2-Y_2O_3 and Ni-Cr-Al-Y in the outer layer above a Ni-Cr-Al-Y bond coat. One cermet coating was applied by low pressure plasma spraying (LPPS) while the second was applied by air plasma spraying (APS). Metal temperatures were measured either below the coating or on the inner wall of the tube. A thermal model was developed to predict temperatures in the coating and substrate for both tube and rod geometries. Use was made of previously measured gas temperatures and heat transfer coefficients for tubes located at the throat of the rocket engine (ref. 3). Using this data, previous modelling work showed good agreement between measured and predicted near-surface metal temperatures in an uncoated tube (ref. 3).

The thermal model was also used to examine the effect of the range in the reported values of the thermal conductivity of plasma sprayed ZrO_2-Y_2O_3 ceramic coatings, the effect of a 100 μm (0.004 in.) thick metallic bond coat, the effect of tangential heat transfer around the tube, and the effect of radiation from the surface of the ceramic coating. Comparing predicted temperature profiles for rod and tube substrates allowed the temperature differences between the two substrates to be quantified.

The effectiveness of the various coatings in reducing the thermal shock to SSME-HPFTP blades was examined by predicting surface temperatures at the leading edge with and without the coatings. This latter study was accomplished by developing a thermal model for the leading edge and using gas temperatures and heat transfer coefficients appropriate for SSME start-up.

EXPERIMENTAL PROCEDURE AND RESULTS

Rocket Engine Operation

The rocket engine is shown schematically in figure 1. Five 0.953 cm (0.375 in.) tubes (or rods) were held in a copper specimen holder such that all gas flow was perpendicular to the cylindrical axis. The hot gas exiting the combustion chamber is constricted by the presence of the tubes located at the throat of the rocket engine. High pressures in the combustion chamber result in Mach 1 exhaust gas velocities slightly upstream from the throat plane (the plane passing through the cylindrical axis of each of the tubes yielding the smallest cross-sectional throat area). The area blockage ratio for the engine, given as $W/(W - D)$ (see fig. 1), is equal to 2.875 giving an area reduction (inverse of the area blockage ratio) at the throat of 0.348.

Only three of the five specimens are fully exposed in the gas flow (positions 2, 3, and 4, fig. 1). However, gas temperature measurements indicated significant temperature differences between these three center test positions. Hence, all testing of thermal barrier coated tubes and rods was performed with test specimens in position 2. Along the length of the tube at position 2, the temperature changed significantly, generally being highest at the midpoint and decreasing toward the rocket chamber walls. Consequently, metal temperatures in the tubes were only measured at the midpoint (lengthwise) of the tube. However, even at the midpoint, the gas temperature varied with angular position around the test tube such that gas temperatures measured near the stagnation point of the tube ($\Theta = 0°$, facing the injector) were significantly greater than gas temperatures measured on the exhaust side of the tube, opposite the injector ($\Theta = 180°$). As a consequence, instrumented tubes were always oriented such that the thermocouples faced the injector ($\Theta = 0°$). Typical gas temperatures for the stagnation point and on the exhaust side of the tube are shown in figure 2. These relatively low gas temperatures were achieved by maintaining a hydrogen-rich environment in the rocket chamber with an oxygen to hydrogen mass ratio of approximately 1.2 to 1.4 (stoichiometric combustion at a mass ratio near eight produces gas temperatures in excess of 3000 °C). Gas temperature measurements are discussed in detail elsewhere (ref. 3).

Standard operation of the engine involved opening the O_2 valve 0.1 sec before opening the H_2 valve which generally ensured engine ignition in the hydrogen-rich environment. The test duration was 1.2 to 1.3 sec. At the end of the test, the O_2 valve was closed 0.3 sec prior to the closing of the H_2 valve which resulted in a short H_2 purge of the test tube. As either the O_2 or the H_2 valve was closed, each line was purged by gaseous N_2 which resulted in a N_2 purge cooling the specimen to room temperature. The pressure in the chamber of the rocket engine was maintained at approximately 2.07 MPa (300 psi). Specimen temperatures before, during and after a test were measured at a frequency of 100/sec. Further details of the rocket engine operation are given in reference 3.

Thermal Barrier Coatings

Traditional TBC's applied at NASA Lewis. - Near-surface metal temperatures were measured at an angular orientation facing the injector on 0.953 cm o.d., 0.648 cm i.d. (0.375 in. o.d., 0.255 in. i.d.) directionally solidified (DS) Mar-M246+Hf tubes[1] coated with a traditional plasma-sprayed ZrO_2-Y_2O_3 TBC. The tubes were instrumented by cutting channels 0.038 cm (0.015 in.) in depth by 0.056 cm (0.022 in.) in width. Individually-sheathed thermocouples, 0.0254 cm (0.010 in.) diameter sheath with 0.0065 cm (0.003 in.) diameter wire, were placed in the channels and the beads welded to the bottom of the channel. The channels were covered with a 0.013 cm (0.005 in.) Inconel 600 sheet which was welded in place to seal the channel from the hot gas. A cross-sectional view of the channel and the individually-sheathed thermocouple wires is shown in figure 3. Prior to coating application, the surface of the instrumented tubes was cleaned and roughened by grit blasting with 60 grit, high-purity alumina at 0.48 MN/m^2 (70 psi) followed by ultrasonically degreasing. The instrumented tubes were then coated with a 25 to 50 μm (0.001 to 0.002 in.) APS Ni-Cr-Al-Y

---

[1] The composition of DS Mar-M246+Hf is Ni-10Co-9Cr-10W-5.5Al-2.5Mo-1.5Ta-1.5Ti-0.15C-0.015B-0.05Zr-1.75Hf wt %.

bond coat layer. Bond coat roughness before top coat application was 12.2 μm RA (481 μin.). The ceramic top coat was plasma sprayed to thicknesses ranging from 100 to 275 μm (0.0045 to 0.0095 in.). Details of the plasma spraying process and initial powder compositions are given in table I and specimen designations, coating thicknesses, and surface roughnesses are given in table II.

Two of the coated tubes were tested in the as-sprayed condition, after which the surface was smoothed by sanding with SiC paper and the coatings were retested. The surface roughness of the as-sprayed coatings and that following sanding is given in table II. It was previously shown that differences in the surface roughness in the ranges shown in table II for as-sprayed and sanded surfaces have little effect on the heat transfer to the tubes (ref. 3). A traditional ZrO_2-Y_2O_3 TBC was also applied in a manner as that given above but on a B-1900 superalloy substrate.[2] A single thermocouple was attached to the inner wall of this tube to permit temperature measurements at the same location as for the cermet coatings, discussed below. The coating designation (TK3) and thickness for this specimen are given in table II.

Post-test microstructures of the traditional TBC's plasma-sprayed at NASA Lewis are shown in cross section in figure 4. The difference in surface roughness after sanding can be seen by comparing the as-sprayed coatings in figures 4(a) and (c) (specimens TN1 and TK1) with the coatings after sanding shown in figures 4(b) and (d) (specimens TN2 and TK2). The nonuniformity in the bond coat thickness is apparent in all four specimens. It appears that large bond coat powder particles were not fully melted during plasma spraying. There also appears to be a significant amount of porosity in the ceramic top coat, especially in the two thicker coatings. Much of this porosity is believed due to pull out during the polishing process even though the specimens were vacuum epoxy impregnated prior to polishing. Some porosity is also apparent in the bond coat which may also be due, in part, to the polishing procedure. APS bond coats can contain significant amounts of oxide resulting in poor adhesion of small particles in the coating.

Cermet coatings. - Two cermet coatings applied by different techniques were tested. The metallic bond coat and cermet layers of one of the coatings were applied by LPPS techniques while both layers for the second coating were applied by APS techniques. The volume fraction of ZrO_2-Y_2O_3 in the APS cermet was approximately 0.33 whereas the volume fraction in the LPPS cermet was approximately 0.47. The tubes for the cermet coatings were instrumented with a single thermocouple attached to the inner wall at the midpoint (lengthwise) of the tube. Coating designations, thicknesses, compositions, and surface roughnesses are given in table III.

The post-test microstructure of the LPPS 50/50CM coating is shown in figure 5(a). The LPPS bond coat is almost indistinguishable from the Mar-M246+Hf substrate. It is also apparent from the microstructure that some of the large Ni-Cr-Al-Y particles in the outer cermet coating were not fully melted during plasma spraying. Some porosity is also apparent in the ZrO_2-Y_2O_3 particles in the cermet layer. Because this porosity is on a much finer scale than that for the traditional TBC's shown in figure 4, it is not apparent whether the

---

[2] The nominal composition of B-1900 superalloy is Ni-10Co-8Cr-6Mo-6Al-4Ta-1Ti-0.1C-0.1Zr-0.015B wt %.

porosity is due, in part, to polishing or was present following plasma spraying. The post-test microstructure of the APS 30/70CM coating is shown in figure 5(b). Oxide stringers, generally parallel to the surface, are apparent in the bond coat and in the cermet coating. These oxide stringers generally result from the metal powder particles developing a thin oxide scale during plasma spraying in air. The molten powder particles impact the surface and "splat" developing the traditional "pancake" or "splat" morphology with the oxide stringers delineating the splat boundaries.

Measured Temperature Profiles

The effectiveness of the traditional TBC's applied at NASA Lewis is apparent in figure 6(a) where the temperature profile for an uncoated tube is compared to representative temperature profiles measured below TBC's of two different thicknesses. The addition of 100 to 125 μm ceramic layer for the TN1 specimen reduced the maximum metal temperature by approximately 350 °C. Surprisingly, increasing the ceramic layer thickness to 200 to 225 μm for the TK1 specimen only resulted in an additional metal temperature reduction of 100 °C. The rapid temperature decrease of the uncoated tube between 6.3 and 6.6 sec occurs during purging with H_2 and the more gradual cooling after 6.6 sec occurs during purging with N_2. Even with the TBC's, the effectiveness of the H_2 purge is apparent.

Representative temperature profiles for the cermet coatings and that for the traditional TBC (specimen TK3) with thermocouples on the inner wall of the tube are shown in figure 6(b). The near-surface temperature profile for the uncoated tube, shown for comparison, indicates that the cermet coatings offer only limited thermal protection.

THERMAL MODELLING ANALYSIS AND RESULTS

Thermal Models for Coated Throat Tubes in the NASA Lewis Rocket Engine

Thermal model development and analysis. - Two finite-difference thermal models were developed to simulate heat transport in coated and uncoated tubes and rods during testing in the rocket engine. The first thermal model simulated convective heat transfer at the stagnation point and accounted for conductive heat transfer in a radial direction only (one-dimensional model). The second thermal model considered convective heat transfer over the surface of the tube from the stagnation point ($\Theta = 0°$) to the exhaust side of the tube ($\Theta = 180°$) and accounted for both radial and tangential conductive heat transfer within the tube wall (two-dimensional model). The two models are shown schematically in figures 7(a) and (b).

The one-dimensional thermal model consisted of a 45° slice which contained 61 nodes for the tube and 86 nodes for the rod. For the tube, the near-surface grid spacing was 12.5 μm (0.0005 in.) and the spacing near the inner wall was 50 μm (0.002 in.). The near-surface grid spacing for the rod was the same as that for the tube increasing to 125 μm (0.005 in.) at the center of the rod. The two-dimensional thermal model consists of a total of 110 nodes and equidistant grid spacing as shown in figure 7(b). The appropriate heat transfer equations for conduction, convection and radiation were solved for both models by the numerical computer program known as SINDA (Systems Improved Numerical

Differencing Analyzer) (ref. 4). The SINDA program allows considerable flexibility, including temperature-dependent thermal conductivities (K(T)), specific heats (Cp(T)), and emissivity values (ε(T)), as well as time-dependent gas temperatures and heat transfer coefficients (h_c). The temperature dependence of K and Cp for the Mar-M246+Hf substrate (ref. 5) is shown in figures 8(a) and (b), respectively, and the density (ρ) of the substrate material (ref. 5) is given in table IV.

The gas temperature used in the one-dimensional model was that for $\Theta = 0°$ (stagnation point), shown in figure 2. A value of 33 kW/m^2 °C was used for the heat transfer coefficient at the stagnation point (ref. 3). During engine start-up, the heat transfer coefficient was scaled with the normalized chamber pressure as $(P_c/P_0)^{0.8}$ (P_0 = 2.07 MPa) to reflect the pressure dependence of the heat transfer coefficient assuming turbulent heat transfer (ref. 3). The resulting time dependence of h_c during the 1.2 sec heating, H_2 purge, and N_2 purge is shown in figure 9(a). These values for h_c were used very successfully to predict near-surface metal temperatures in an uncoated Mar-M246+Hf tube during testing in the rocket engine (ref. 3).

The convergence of the numerical solution was initially verified with the one-dimensional model by varying the number of nodes and thereby changing the grid spacing. Temperature profiles through the wall of an uncoated tube were predicted with 16 and 30 nodes and compared to the predictions using 61 nodes. The grid spacing near the surface with both 16 and 30 nodes was 25 µm whereas the spacing was 125 µm at the inner wall with 30 nodes and 500 µm with 16 nodes. Temperatures throughout the tube wall differed by less than 1 °C when the number of nodes was reduced from 61 to 30. However, when the number of nodes was reduced to 16, surface temperatures were up 9° higher while inner wall temperatures were up to 41 °C lower. Hence, the grid spacing resulting from using 30 or more nodes was sufficient to produce a convergent solution.

The possibility of tangential heat flow reducing the stagnation point temperatures, where metal temperatures were measured, was examined with the two-dimensional thermal model. Figure 2 shows that the measured gas temperatures on the exhaust side of the tube ($\Theta = 180°$) were significantly lower than those at the stagnation point. In addition, results from reference 3 indicate that the heat transfer coefficient decreases in value from the stagnation point to the exhaust side of the tube, as shown in figure 9(b). This combination of high gas temperatures and high heat transfer coefficients at the stagnation point, and conversely, low gas temperatures and low heat transfer coefficients on the exhaust side of the tube would be expected to produce much higher metal temperatures at the stagnation point than on the exhaust side of the tube. This difference in metal temperatures could result in significant tangential heat transfer within the tube wall reducing the metal temperature at the stagnation point where temperature measurements on coated tubes were made. However, measured gas temperatures and heat transfer coefficients at $\Theta = \pm 90°$ are similar to those at the stagnation point (ref. 3) which should reduce any impact at the stagnation point of tangential heat flow to the exhaust side of the tube. Additionally, the heat transfer coefficients decrease significantly at approximately $\Theta = \pm 130°$ where flow separation occurred (ref. 3), such that any large temperature gradients in the tangential direction would be expected near this region.

The maximum effect of the tangential heat flow was evaluated with the two-dimensional model by considering an uncoated tube and using gas temperatures for $\Theta = \pm 0°$ (fig. 2) at nodes between angles 0° and 150° and the lower gas temperatures for $\Theta = 180°$ (fig. 2) for nodes between 150° and 180°. Values for h_c at the 10 surface nodes around the tube were taken from figure 9(b).

The two-dimensional thermal model was run with and without tangential heat flow. Predicted surface temperatures around the tube after 0.3, 0.6 and 1.2 sec, accounting for tangential heat flow, are shown in figure 10(a). As expected, the surface temperature at the stagnation point ($\Theta = 0°$) rises more rapidly than that on the exhaust side of the tube ($\Theta = 180°$), rising to more than 80 percent of the maximum temperature after only 0.3 sec. The predicted time dependence of the surface temperature at $\Theta = 0°$ and at $\Theta = 180°$, with and without tangential heat flow, are shown in figure 10(b). There is less than 10 °C reduction in the stagnation point temperature ($\Theta = 0°$) when tangential heat transfer is taken into account. However, on the exhaust side of the tube ($\Theta = 180°$), heat flow around the tube to the exhaust side increases the temperature approximately 140 °C. Hence, tangential heat flow does not significantly reduce the stagnation point temperature but does substantially increase the temperature on the exhaust side of the tube ($\Theta = 180°$). Therefore, in comparing measured and predicted stagnation point temperatures for tubes tested in the NASA Lewis rocket engine, the one-dimensional thermal model (45° wedge facing the injector) was considered adequate for predicting temperatures within the scatter in the measured temperature data.

The effect of the range in the reported values of the thermophysical properties of ZrO_2-Y_2O_3 ceramic coatings was examined with the one-dimensional model. Several reported values of the temperature dependence for the thermal conductivity (K) and the specific heat (Cp) for APS ZrO_2-Y_2O_3 are shown in figures 11(a) and (b). The effect of this range in the values for K was examined by predicting temperature profiles for a 180 µm (0.007 in.) thick ceramic layer on a Mar-M246+Hf tube. Two cases with different values for K and Cp for APS ZrO_2-Y_2O_3 were considered. For Case I, values for K reported in reference 6[3] (curve 12, fig. 11(a)) and values for Cp reported in reference 7 (curve 10, fig. 11(b)) were used (values for Cp were not reported in ref. 6). For Case II, values for K and Cp reported in reference 8 (curve 9, figs. 11(a) and (b)) were used. These values for K were chosen as a lower bound (Case I) and as an upper bound (Case II) for the reported data (fig. 11(a)). The values for Cp for both cases are nearly identical (fig. 11(b)). Identical K and Cp data for the Mar-M246+Hf substrate were used. The predicted temperatures for the surface of the ceramic and at the ceramic-metal interface (tube surface) are shown in figure 12. Figure 12 shows that the range in the values of the thermal conductivity amounts to less than a 50 °C difference in the predicted ceramic surface temperature. However, the predicted temperatures vary by 180 °C at the ceramic/metal interface. Hence, the range in the reported values for K for APS ZrO_2-Y_2O_3 coatings result in significant temperature differences at the ceramic/metal interface and moderate temperature differences on the surface of the ceramic.

---

[3] Reference 6 gives a regression equation fitting data from several sources including data for ZrO_2-Y_2O_3 TBC's applied by electron beam, physical vapor deposition (EB-PVD). However, as shown in this reference, little difference is observed in the reported thermal conductivity between the APS and EB-PVD coatings.

Radiation from the ceramic coating reduces the temperature of the surface. Liebert (ref. 9) has reported correlation equations for the emissivity for several thicknesses of APS ZrO_2-Y_2O_3 TBC's in the temperature range 27 to 2500 °C. For a 180 μm (0.007 in.) thick coating, the work by Liebert suggests a nearly decreasing value of the emissivity from 0.96 at 27 °C to 0.46 at 1500 °C. These emissivity values were used in the thermal model to evaluate the reduction in surface temperature due to radiative heat losses. This effect amounted to less than a 10 °C decrease at the surface of the ceramic coating and an almost negligible decrease at the ceramic/metal interface. Hence, it is not necessary to account for radiative heat losses from the ceramic coating during the short duration testing used in this study.

Most TBC's are fabricated with a metallic bond coat layer between the ceramic layer and the substrate. These bond coat layers are typically 75 to 125 μm (0.003 to 0.005 in.) thick and may be plasma sprayed in air (APS) or at reduced oxygen pressures (LPPS). The thermal conductivity of various reported bond coats, both APS and LPPS, are shown in figure 8(a). It is apparent that LPPS bond coats exhibit a much higher thermal conductivity than APS bond coats, and generally exceed that for the Mar-M246 substrate. The lower values for the APS bond coats can generally be attributed to the amount of oxide present in these coatings.

The effect of the presence of a bond coat on the temperatures in the substrate was evaluated by modelling a TBC with a 180 μm (0.007 in.) ceramic top coat above a 100 μm (0.004 in.) metallic bond coat. The effect of differences in the reported values of the thermophysical properties of metallic bond coats was examined by again considering two cases. In Case I, values for K reported in reference 10 for an APS Ni-Cr coating (curve 2, fig. 8(a)) and values for Cp reported in reference 7 for an APS Ni-Cr-Al coating (curve 3, fig. 8(b)) were used. In Case II, values for K and Cp reported in reference 8 for an APS Ni-Cr-Al-Y coating (curve 1, figs. 8(a) and (b)) were used. At high temperatures, the values for K for Case I are double those for Case II (compare curves 1 and 2, fig. 8(a)). Figure 13 shows the predicted near-surface temperatures for the two cases as well as predicted temperatures without a bond coat present. For case I, with a thermal conductivity closer to that of the Mar-M246+Hf substrate, the temperature in the substrate is reduced by a maximum of only 10 °C while for case II, with a lower reported thermal conductivity, the temperature in the substrate is reduced by approximately twice this amount. In the ceramic coating, temperatures increased but by smaller amounts than the decreases in the substrate. Since values for K for LPPS coatings are generally greater than that for Mar-M246+Hf (fig. 8(a)), the presence of LPPS bond coats would be expected to have a negligible effect on the temperatures in the substrate or the ceramic coating. Hence, accounting for the presence of the bond coat layer between the substrate and the ceramic top coat makes only a small difference in the predicted temperatures in either the ceramic layer or the substrate.

The difference in the thermal response between a tube and rod was examined by predicting temperature profiles for both substrate geometries with 100 and 200 μm (0.004 and 0.008 in.) thick ceramic coatings. The gas temperature and heat transfer coefficient used in this comparison were those for $\theta = 0°$ (see figs. 2 and 9(a)). Thermophysical properties and density for the Mar-M246+Hf substrate are as given in figures 8(a) and (b) (curve 13) and table IV. Because of the range in the reported values for K for ZrO_2-Y_2O_3 coatings, median values were used (see fig. 11(a)). Values for Cp were taken from reference 7 (curve 10, fig. 11(b)) and a value of 4.8 gm/cm^3 was chosen as a typical density (table IV). The temperatures predicted on the surface of the ceramic layer and at the ceramic/metal interface for both the tube and rod geometry are shown in figure 14(a). As shown, there is very little difference between the tube and rod in the surface temperature of the ceramic where, after 1.2 sec, the rod was 34 °C lower than the tube for the thinner coating and 16 °C lower than the tube for the thicker coating. More significant differences are apparent at the ceramic/metal interface. At this interface, the temperature for the rod is 160 °C lower than the tube for the 100 μm (0.004 in.) coating and approximately 145 °C lower than the tube for the 200 μm (0.008 in.) coating. Figure 14(a) also shows that the temperature at the surface of the coating and at the coating/metal interface increases slightly faster for the tube than that for the rod during the steady state gas temperature region between 5.5 and 6.2 sec (see also fig. 2). This result simply reflects the greater thermal mass of the rod. Hence, for the same gas temperature, the metal surface temperature of the rod is approximately 150 °C lower than that for the tube.

It is also interesting to examine the temperature differences due to the coating thickness as shown in figure 14(a). A temperature difference of 60 °C exists at the ceramic surface of the two coatings after 0.3 sec, regardless of the geometry. However, temperature differences for the two coating thicknesses are greater at the ceramic/metal interface where, for the tube, this difference due to the coating thickness is 232 °C, and for the rod, the difference is 216 °C. For comparison, the predicted temperature of the surface of an uncoated Mar-M246+Hf tube after 1.2 sec, under the same conditions, is 1374 °C (ref. 3). Hence, the predicted benefit of a 100 μm (0.004 in.) TBC in reducing the metal temperature for the tube substrate is 294 °C and the benefit of a 200 μm (0.008 in.) TBC is 526 °C. As expected, the predicted temperature benefit is not directly proportional to the TBC thickness.

Radial temperature profiles through a 200 μm (0.008 in.) thick coating and into rod and tube substrates are shown in figure 14(b). Simply by considering the area under the temperature profile for each substrate shows that the rod acts as a greater heat sink than the tube. It appears that the temperature across the ceramic coating decreases linearly. However, a close examination of the temperatures indicates a slight concave downward curvature consistent with a nearly-constant surface temperature (see fig. 14(a)) and a slightly increasing thermal conductivity for the ceramic layer (see fig. 11(a)). As the surface temperature rises at short times (<0.1 sec), the temperatures in the ceramic layer exhibited a slightly concave upward curvature, as expected during the early heat-up period.

Predicting metal temperatures in throat tubes. - The 61 node one-dimensional tube model was used to predict temperatures in the NASA Lewis-applied TBC's and the APS 30/70CM and LPPS 50/50CM coatings. Based on the previous modelling results, the presence of a metallic bond coat and radiative heat losses from the surface of the coatings were not considered. The gas temperature and heat transfer coefficient used in this study were those for $\theta = 0°$ (figs. 2 and 9(a)). Thermophysical properties and density for the DS Mar-M246+Hf substrate are as given in figures 8(a) and (b) (curve 13) and table IV. Median values for K for the ZrO_2-Y_2O_3 coating were again used (fig. 11(a)). Values for Cp were taken from reference 7 (curve 10, fig. 11(b)) and a value of 4.8 gm/cm^3 was chosen as a typical density (table IV). Because of the similarity in values (ref. 11), the thermal conductivity, specific heat, and density of Mar-M246+Hf was used for the B-1900 substrate (specimen TK3). The coating thicknesses of 100, 140, 200, and 250 μm were chosen to span the measured coating thicknesses (table II). The measured and predicted temperatures 0.0381 cm (0.015 in) below the ceramic/metal interface for specimens TK1 and TK2 (200 and 250 μm thick coatings) are shown in figure 15(a) and for the TN1 and TN2 (100 and 140 μm thick coatings) in figure 15(b). The measured and predicted inner wall temperatures for the TK3 specimen (250 μm thick coating) are shown in figure 15(c). The cooling period associated with the H_2 purge (6.2 to 6.5 sec) is predicted somewhat sooner than actually observed. This difference in the onset of cooling may indicate the finite time required for the O_2 valve to close and for the H_2 purge to actually begin. The measured temperature profiles indicate that the hot gas may be present in the chamber for approximately 0.1 sec longer than the value used in modelling (i.e., an actual hot test duration of 1.3 sec). However, in considering the range in the reported values for the thermal conductivity of the ceramic layer, the agreement between the measured and predicted temperatures is quite good.

The temperature dependence of K and Cp for the cermet coatings is given in figures 8(a) and (b), respectively. Average values for the coating thicknesses of 64 μm (0.0025 in.) for the LPPS 50/50CM and 180 μm (0.007 in.) for the APS 30/70CM coatings (see table III) were used in the model. Measured and predicted inner wall temperatures for these two coatings are shown in figures 16(a) and (b). Again, the agreement is quite reasonable considering the number of potential sources of uncertainty.

Potential Benefit of TBC's on HPFTP Blades

Thermal model development. - A thermal model was developed to predict heat transfer to the leading edge (LE) of an HPFTP blade during start-up of the SSME. The leading edge was selected because heat transfer coefficients in this region are predicted to be greater than for other parts of the blade (ref. 12). This LE thermal model approximated the leading edge with a cylinder, the radius of the cylinder being equal to the radius of curvature of the leading edge of the blade near the blade tip (radius = 0.0762 cm (0.03 in.)). Only heat transfer to the stagnation point of the leading edge was considered. Similar to the one-dimensional model of the rod, the LE thermal model used a 45° wedge from the cylinder to simulate heat transfer at the stagnation point and consisted of a minimum of 20 nodes with a grid spacing of 0.0051 cm (0.002 in.) near the cylinder center, 0.0025 cm (0.001 in.) near the metal surface, and 0.00127 cm (0.0005 in.) in the coating. Coating thicknesses of 64 and 165 μm (0.0025 and 0.0065 in.) were considered. The LE model also utilized the SINDA thermal differencing analyzer to solve the appropriate differential equations. The model is shown schematically in figure 17.

The gas temperature profile for the HPFTP during engine start-up and the heat transfer coefficients predicted for the stagnation point of the leading edge are shown in figure 18 (refs. 12 and 13). The heat transfer coefficient during the first thermal excursion is low because of low pressures in the HPFTP preburner and low rotational velocities for the turbine wheel. Values for K, Cp and ρ for Mar-M246+Hf were taken from figures 8(a) and (b) and table IV.

Predicted temperatures. - The ability of numerous coatings to reduce the thermal transients at the leading edge of an HPFTP blade was examined. The range in the values for K for the traditional ZrO_2-Y_2O_3 TBC's was examined by again taking the data reported in reference 6 as a lower bound and the data reported in reference 8 as an upper bound (see fig. 11(a)). Both cermet coatings were also examined as well as an APS Ni-Cr-Al-Y metallic coating using data for K and Cp reported in reference 8 (curve 1, figs. 8(a) and (b)). The temperature dependent thermophysical properties (K and Cp) for each of these coatings, as shown in figures 8 and 11, were used in the LE thermal model.

Predicted temperature profiles at the coating/metal interface for each of the 165 µm (0.0065 in.) thick coatings are shown in figure 19. The surface temperature for an uncoated blade is shown for comparison. It is apparent that significant temperature reductions (>100 °C) can be achieved with any of the coatings. Temperature reductions are somewhat greater for the first thermal excursion, however, the proportionate reduction for both thermal excursions is similar. The maximum metal temperature at the first and second thermal excursion is shown in figure 20(a) for the 165 µm (0.0065 in.) thick coatings and figure 20(b) for the 64 µm (0.0025 in.) thick coatings.

DISCUSSION

The measured temperature profiles for the TN1 and TK1 specimens (see fig. 6(a)) indicate the significant potential of TBC's to reduce metal temperatures during short thermal excursions. These temperature profiles indicate that a temperature reduction of approximately 350 °C can be realized with only a 100 to 125 µm thick TBC layer. It is somewhat surprising that almost doubling the thickness of the TBC to 200 to 225 µm only reduces the temperature by an additional 100 °C. The predicted temperature profiles for the two coating thicknesses shown in figure 14(a) would indicate that a larger temperature reduction would be expected on doubling the coating thickness. Since temperature changes are governed by the nonsteady state heat equation and not a simple linear or inversely linear relationship, doubling the coating thickness does not double the thermal protection. Most likely, the smaller than expected temperature reduction can be attributed to the uncertainty in the coating thicknesses above the thermocouples (see table II).

The measured temperature profiles for the cermet coatings (see fig. 6(b)) indicate very little thermal protection is afforded by these coatings. However, the thermophysical properties of these coatings, specifically the thermal expansion, should be intermediate between that of the substrate or metallic bond coat and a ceramic coating layer. The difference in thermal expansion between a substrate and ceramic coating is believed to be a major cause of spallation of the ceramic layer during thermal cycling of TBC's (ref. 14). The cermet layer may, therefore, be a useful transition layer between the substrate and ceramic top coat. As a practical consideration, the cermet coating must remain relatively thin so as not to add undue weight to the blade. The LPPS cermet coatings show that relatively thin coatings can be applied with thickness uniformity, at least to the simple substrate geometries examined in this study.

Thermal modelling allows the effect of various model configurations (e.g., rod versus tube, with and without a bond coat) and uncertainties in the values of the thermophysical properties (e.g., K(T)) to be examined and quantified. For a 100 μm (0.004 in.) APS metallic bond coat, where the reported values for K differ by more than a factor of two, it was shown that the substrate temperatures were reduced by only a maximum of 10 to 20 °C while temperatures in the ceramic increased even less. This limited effect of the bond coat layer is expected by considering the overall thermal resistance of the TBC which is simply the sum of the thermal resistance for each layer (ceramic and bond coat). Since the thermal resistance is inversely proportional to the thermal conductivity, the thermal resistance of the ceramic (low K) outweighs that for the bond coat for similar layer thicknesses. The relatively high thermal conductivity of LPPS bond coats, similar to that of the Mar-M246+Hf substrate, results in very little thermal resistance and would produce little effect on temperatures in the substrate.

The uncertainty (approximately ±50 percent) in the reported values for the thermal conductivity of the APS ZrO_2-Y_2O_3 ceramic layer has a significant effect on the predicted substrate temperatures and, to a lesser extent, the temperature in the ceramic layer itself. It is not known whether the differences in the values for K are solely due to variations in the ceramic material (e.g., extent of porosity and microcracking, etc.) or to differences in the measuring techniques. The small differences in the composition of the APS ZrO_2-Y_2O_3 ceramic cannot account for the differences in K. The data reported in reference 6 indicates only small differences between coatings applied by air plasma spraying (APS) and coatings applied by electron beam, physical vapor deposition (EB-PVD), even though the two techniques result in greatly differing microstructures and somewhat different compositions. Thermal conductivity measurements of plasma sprayed ceramics are generally made by either laser flash or steady state comparator techniques, both of which involve difficulties. Similarly, for bond coat materials, there is also a significant difference between the values for K and ρ reported in reference 8 and that reported in references 7 and 15 which cannot be attributed to the compositional differences. For instance, the LPPS Ni-Cr-Al-Y bond coats reported in reference 8 exhibit negligible porosity (see the LPPS bond coat below the LPPS 50/50CM cermet coating in fig. 5(a)), yet the reported density of these coatings is more than 25 percent less, and the values for K are more than 50 percent less than that reported for other LPPS Ni-Cr-Al-base coatings (table IV). Hence, additional thermophysical property measurements accompanied by better coating characterization are required to resolve the somewhat large differences in the properties of seemingly similar coatings. However, the good agreement between the measured and predicted temperatures for the NASA Lewis-applied TBC's suggests that thermal modelling of these TBC's can be successfully performed using median values for K.

Modelling the thermal response of a coated rod and comparing it to that of a coated tube allows the temperature difference due to the greater thermal mass of the rod to be quantified. In past durability testing of TBC's in the rocket engine, coated rods were tested at gas temperatures estimated to be 150 to 200 °C greater than that for the coated tubes. Even at this greater temperature, the coating lives on the rods were generally greater than those for the tubes. The results presented in figure 14(a) show that at the same gas temperature, the temperature at the ceramic/metal interface is 145 to 160 °C lower for the rod than for the tube. Temperature profiles in a coated rod were also predicted for higher gas temperatures. For a 100 μm (0.004 in.) thick TBC, these predictions show that the gas temperature for the coated rod must be 250 °C greater than that for the coated tube in order to produce similar metal surface temperatures for both substrate geometries. Likewise, for a 200 µm (0.008 in.) thick coating, the gas temperature for the coated rod must be increased 310 °C over that for the coated tube to produce similar metal surface temperatures.

One possible explanation for the increased durability of TBC's on the rod substrates during durability testing (ref. 2) can be understood by considering the stresses which develop between the TBC and the substrate. Spalling of the ceramic layer is believed due to differences in thermal expansion between the ceramic layer and the underlying metallic substrate. Generally, a stress free temperature is defined as the temperature of the substrate during application of the ceramic layer. Cooling a coated component below this stress free temperature results in a compressive load on the ceramic and tensile load on the metallic bond coat. Testing at temperatures above the stress free temperature results in a tensile load on the ceramic layer while the bond coat, constrained by the ceramic layer, is compressively loaded. High temperatures at the ceramic/metal interface which occur during testing can allow the relatively soft metallic bond coat to plastically deform by thermally-activated processes to reduce the compressive stress. The consequence of any relaxation by the bond coat is that the stress free temperature increases. Higher bond coat temperatures allow the bond coat to deform more easily and result in a higher stress free temperature. Upon cooling, this increase in the stress free temperature causes a greater compressive stress on the ceramic layer which can result in cracking and spalling of the layer. Hence, the higher ceramic/metal interface temperatures encountered by the tube in comparison to that by the rod can explain the shorter TBC lives on the tube substrates.

There is also some evidence that the TBC's can spall during heating in a high heat flux environment, even during the first thermal cycle (ref. 2). In this case, the higher ceramic/metal interface temperatures produce a greater stress at this interface due to the thermal expansion mismatch. This increased stress may cause sufficient damage within the TBC to result in spalling.

The good agreement between the predicted and measured temperatures for each of the various TBC's verifies the ability of the thermal model to simulate heat transfer to coated throat tubes during short thermal excursions. Good agreement was observed at locations near the ceramic/metal interface and at the inner wall of the tube. For the temperatures at the ceramic/metal interface (figs. 15(a) and (b)), the predicted temperatures maximize 0.1 to 0.2 sec before the measured temperatures. This difference is due to the instantaneous temperature decrease in the gas temperature profile used in the thermal model (see fig. 2.). Although the oxygen valve begins to close after 1.2 sec, the valve does not close instantaneously and a finite time is required for removal of the hot gas from the combustion chamber. It appears that a slightly longer hot fire duration along with a somewhat more gradual temperature decrease would be closer to the actual hot gas temperature profile. However, the good agreement justifies the use of the measured thermophysical property data for each of the coatings and the use of thermal models to predict heat transfer during short thermal excursions.

The predicted temperature reductions for coated HPFTP blades (figs. 19 and 20(a) and (b)) indicate the tremendous potential of TBC's to reduce metal temperatures during the thermal excursions associated with the start-up of the SSME. As expected, the temperature decreases are ordered according to the thermal conductivity with the largest decrease associated with the lowest thermal conductivity. For the 165 μm (0.0065 in.) thick coatings, the temperature reductions for the first thermal excursion vary from approximately 150 °C for the LPPS 50/50CM coating to 470 °C for ZrO_2-Y_2O_3 TBC's using the thermal conductivity data reported in reference 6. The temperature reduction for the APS ZrO_2-Y_2O_3 TBC's using the thermal conductivity data reported in reference 8 is approximately 335 °C, 135 °C less than that using the data reported in reference 6, even though the APS ZrO_2-Y_2O_3 coatings are essentially identical in composition. As previously discussed, this difference indicates the need for additional thermal conductivity data for plasma sprayed coatings and a better understanding of the parameters which affect the thermal conductivity of plasma sprayed coatings. However, even though significant differences exist in the reported values for the thermal conductivity and predicted temperatures, the results shown in figures 20(a) and (b) indicate the significant potential of TBC's to reduce the thermal shock to the blades in the HPFTP.

SUMMARY AND CONCLUSIONS

Traditional APS $ZrO_2Y_2O_3$ TBC's and APS and LPPS cermet coatings were tested in a H_2/O_2 rocket engine located at NASA Lewis. The traditional ZrO_2-Y_2O_3 TBC's showed considerable metal temperature reductions during testing in the hydrogen-rich environment. The thermal response during testing of each of the coatings has been successfully modelled. Good agreement was observed between predicted and measured temperatures at the inner wall of the tube and in the metal near the coating/metal interface.

The thermal model was also used to examine the effect of the difference in the reported values of the thermal conductivity of plasma sprayed ZrO_2-Y_2O_3 ceramic coatings, the effect of a 100 μm (0.004 in.) thick metallic bond coat, the effect of tangential heat transfer around the tube, and the effect of radiation from the surface of the ceramic coating. It was shown that for the short duration testing in the NASA Lewis rocket engine, radiation from the ceramic coating, tangential heat transfer within the tube wall, or the presence of a 100 μm (0.004 in.) bond coat do not significantly affect the predicted metal temperatures. However, the difference in the reported values for the thermal conductivity of traditional APS ZrO_2-Y_2O_3 TBC's can amount to significantly different temperatures (>100 °C) predicted in the tube. The thermal model was also used to predict the thermal response of a coated rod and compared to that for a coated tube. Results from this comparison yield the difference in the metal temperatures for the two substrate geometries which can be used to explain the increased life of coatings on rods in comparison to tubes.

A thermal model was also developed to predict heat transfer to the leading edge of HPFTP blades during engine start-up. The ability of various TBC's to reduce metal temperatures during two thermal excursions was predicted. Temperature reductions of 150 to 470 °C were predicted for 165 μm (0.0065 in.) thick coatings for the larger of the two thermal excursions.

Specific conclusions for this study are:

1. Traditional APS ZrO_2-Y_2O_3 TBC's significantly reduce metal temperatures during short thermal excursions. However, APS and LPPS cermet coatings reduce metal temperatures to a much lesser extent than traditional TBC's under the same test conditions.

2. Thermal models using median values of the thermal conductivity of APS ZrO_2-Y_2O_3 TBC's were used to predict successfully metal temperatures below NASA Lewis-applied APS ZrO_2-Y_2O_3 TBC's during testing in the H_2/O_2 rocket engine at NASA Lewis.

3. Thermal models based on finite-difference techniques were successfully used to predict metal temperatures below ZrO_2-Y_2O_3/Ni-Cr-Al-Y cermet coated tubes tested in the NASA Lewis rocket engine.

4. Based on the successful modelling efforts stated in conclusions 2 and 3 above using available thermophysical data for various TBC's, further modelling results indicate significant temperature reductions (>100 °C) can be achieved at the leading edge of HPFTP blades during the thermal excursions which occur on SSME start-up.

ACKNOWLEDGMENTS

The author would like to thank R.R. Holmes of NASA Marshall Space Flight Center, Huntsville, AL, and T.N. McKechnie of Rocketdyne Division of Rockwell International, Huntsville, AL, for supplying the LPPS ZrO_2-Y_2O_3/Ni-Cr-Al-Y cermet coatings.

REFERENCES

1. Holmes, R.R.: Vacuum Plasma Coatings for Turbine Blades. Advanced High Pressure O_2/H_2 Technology, S.F. Morea and S.T. Wu, eds., NASA CP-2372, 1985, pp. 74-90.

2. Brindley, W.J.; and Nesbitt, J.A: Durability of Thermal Barrier Coatings In a High Heat Flux Environment. Advanced Earth-To-Orbit Propulsion Technology 1988, R.J. Richmond and S.T. Wu, eds., NASA Marshall, 1988, Vol. 1, pp. 661-674.

3. Nesbitt, J.A.; and Brindley, W.J: Heat Transfer to Throat Tubes In a Square-Chambered Rocket Engine at NASA LeRC. NASA TM-102336, 1989.

4. Fink, L.C.: SINDA-Systems Improved Numerical Differencing Analyzer. Available through Computer Software Management and Information Center (COSMIC), The University of Georgia, Athens, GA, 30602, Program MSC 18597.

5. Chandler, W.T.: Materials for Advanced Rocket Engine Turbopump Blades. (RI/RD83-207, Rockwell International Corp., NASA Contract: NAS3-23536) NASA CR-174729, 1983.

6. Strangman, T.E.; Neumann, J.; and Liu, A: Thermal Barrier Coating Life-Prediction Model Development. NASA CR-179648, 1987.

7. Brandt, R., et al.: Specific Heat and Thermal Conductivity of Plasma Sprayed Yttria-Stabilized Zirconia and NiAl, NiCr, NiCrAl, NiCrAlY, NiCoCrAlY Coatings. High Temp.-High Pressures, vol. 18, no. 1, 1986, pp. 65-77.

8. Holmes, R.R.; and McKechnie, T.N.: Vacuum Application of Thermal Barrier Plasma Coatings. Advanced Earth-to-Orbit Propulsion Technology, 1988, R.J. Richmond and S.T. Wu., eds., NASA CP-3012, 1988, Vol. 1, pp. 692-702.

9. Liebert, C.H.: Emittance and Absorptance of the National Aeronautics and Space Administration Ceramic Thermal Barrier Coating, Thin Solid Films, vol. 53, no. 2, 1978, pp. 235-240.

10. Wilkes, K.E.; and Lagedrost, J.F.: Thermophysical Properties of Plasma Sprayed Coatings. NASA CR-121144, 1973.

11. Aerospace Structural Metals Handbook, Battelle Laboratories, Columbus, OH, 1988.

12. Abdul-Aziz; Tong, M.T.; and Kaufman, A.: Thermal Finite-Element Analysis of Space Shuttle Main Engine Turbine Blade. NASA TM-100117, 1987.

13. Abdul-Aziz: Private Communication. (This data was summarized in the publication given in ref. 12.)

14. Miller, R.A.: Current Status of Thermal Barrier Coatings - An Overview. Surf. Coat. Technol., vol. 30, no. 1, 1987, pp. 1-11.

15. DeMasi, J.T.: Thermal Barrier Coating Life Prediction Model Development. NASA CR-179508, 1986.

TABLE I. - PLASMA SPRAYING PARAMETERS FOR NASA LEWIS COATINGS

[Environment, 0.10-MN/m^2 (1-atm) air; arc gas, 23-liter/min argon; plasma gun, EPI 120-kW plasma generator (#167 anode, #27 cathode, 0.040 stainless steel powder port).]

Parameter	Bond coat	Ceramic top coat
Composition, wt %	Ni-35.8Cr-6.3Al-0.96Y	ZrO_2-6.8Y_2O_3
Tube rotation, rpm		
Plasma gun:		
Power, kW	14	48
Traverse speed, mm/s	30	10
Number of passes	2	[a]6 to 9
Standoff distance (gun to specimen), cm (in.)	11.4 (4.5)	10.2 (4)
Power feeder:		
Rotation, rpm	0.8	2.0
Gas, liter/min	Ar, 2.4	Ar, 1.6

[a] Depending on desired thickness.

TABLE II. - THERMAL BARRIER COATINGS APPLIED AT NASA LEWIS

Coating designation[a]	Bond coat thickness[b]		Ceramic coat thickness[b]		Surface roughness (RA)[c]	
	μm	in.x10^{-3}	μm	in.x10^{-3}	μm	μin.
Before sanding						
TN1	25 to 50	1 to 2	100 to 125	4 to 5	9.4	372
TN2	(d)	(d)	(d)	(d)	10	395
TK1	25 to 50	1 to 2	200 to 225	7.9 to 8.8	9.3	365
TK2	(d)	(d)	(d)	(d)	9.6	378
TK3[e]	50 to 75	2 to 3	225 to 275	8.8 to 10.8		
After sanding						
TN2	25 to 75	1 to 3	100 to 140	4 to 5.5	3.2	127
TK2	25 to 50	1 to 2	200 to 250	7.9 to 9.8	5.1	200

[a] TN refers to coatings with a thinner ceramic top coat, TK refers to coatings with a thicker ceramic top coat.

[b] Measured from cross sections after testing.

[c] Average of four measurements.

[d] Unmeasured prior to sanding.

[e] B-1900 superalloy substrate.

TABLE III. - CERMET THERMAL BARRIER COATINGS

	Coating designation	
	LPPS 50/50CM[a]	APS 30/70CM[b]
Bond coat thickness,[c] μm (in.x10^{-3})	50 (2)	40 to 60 (1.6 to 2.4)
Cermet coat thickness,[c] μm(in.x10^{-3})	50 to 75 (2 to 3)	150 to 200 (6 to 8)
Surface roughness (RA), μm (μin.)	5.3 (210)	9.4 (372)
Volume fraction of oxide	0.47±0.12	0.33±0.10
Composition (wt %):[d]		
Metal (in bond coat and cermet)	Ni-16.5Cr-5.5Al-0.55Y	Ni-16.5Cr-5.5Al-0.55Y
Ceramic (in cermet)	ZrO_2-8Y_2O_3	ZrO_2-8Y_2O_3

[a] Low-pressure, plasma-sprayed bond coat and cermet coat (approx. 50 percent ceramic, 50 percent metal in cermet coat). Applied by NASA Marshall Space Flight Center, Huntsville, AL.

[b] Air-plasma-sprayed bond coat and cermet coat (approx. 30 percent ceramic, 70 percent metal in cermet coat). Applied by Plasma Coating Corporation, Gardina, GA.

[c] Measured from cross sections after testing.

[d] Taken from reference 8.

TABLE IV. - DESIGNATION AND DENSITY OF COATINGS AND SUBSTRATE

Designation[a]	Density, ρ, g/cm^3	Reference
APS metallic coatings:		
1 Ni-Cr-Al-Y	4.48	8
2 Ni-Cr	6.8	10
3 Ni-Cr-Al	6.9	7
LPPS metallic coatings:		
4 Ni-Cr-Al-Y	5.48	8
5 Ni-Cr-Al	7.48[b]	7
6 Ni-Co-Cr-Al-Y	-----	15
Cermet coatings:		
7 LPPS 50/50CM	4.55	8
8 APS 30/70CM	4.01	8
APS ceramic coatings:		
9 ZrO_2-$8Y_2O_3$	3.47	8
10 ZrO_2-(7 to 8)Y_2O_3	5.39[c]	7
11 ZrO_2-$7Y_2O_3$	4.5[d]	14
12 ZrO_2-Y_2O_3[e]	-----	6
Substrate:		
13 DS Mar-M246+Hf	8.6	5

[a] Number used to identify substrate and coating in figures 8, 11, 19, and 20.

[b] Average for three different LPPS Ni-Cr-Al-based metallic coatings.

[c] Representative values for several reported APS ZrO_2-(7 to 8)Y_2O_3 coatings.

[d] Based on reported 20 percent porosity.

[e] Regression fit of data from several sources includes data for ZrO_2-Y_2O_3 coatings applied by electron-beam, physical vapor deposition.

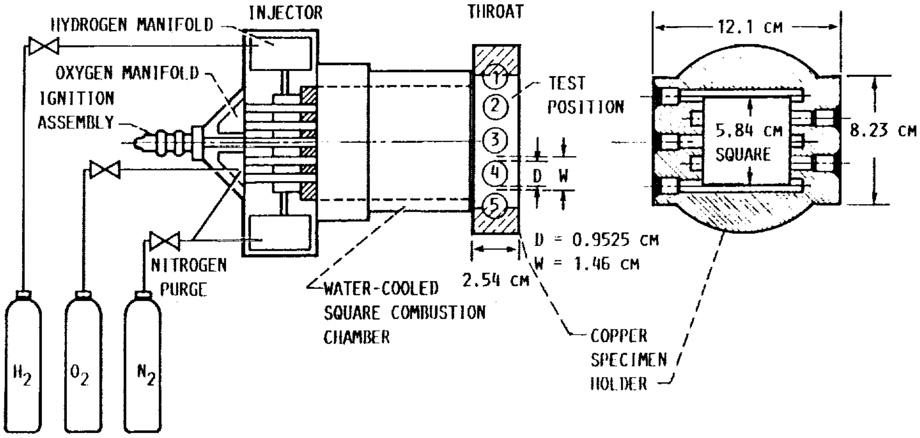

FIGURE 1. - SCHEMATIC VIEW OF THE ROCKET ENGINE AND COPPER SPECIMEN HOLDER.

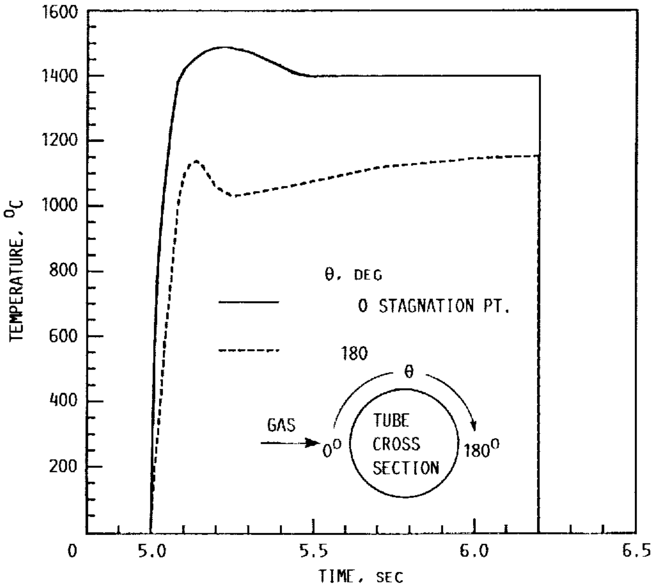

FIGURE 2. - GAS TEMPERATURE PROFILES AT THE STAGNATION POINT ($\theta = 0^\circ$) AND AT THE EXHAUST SIDE ($\theta = 180^\circ$) OF TEST POSITION 2 NEAR THE TUBE MIDPOINT (LENGTHWISE) (REF. 3).

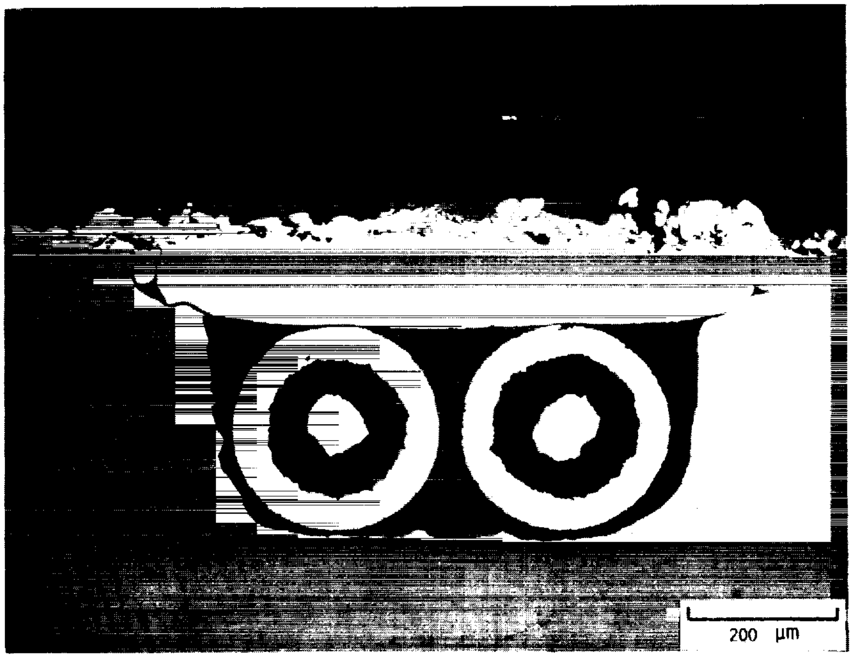

FIGURE 3. - CROSS-SECTIONAL VIEW OF THE NEAR-SURFACE THERMOCOUPLES BELOW A TRADITIONAL ZrO_2-Y_2O_3 TBC.

ORIGINAL PAGE
BLACK AND WHITE PHOTOGRAPH

ORIGINAL PAGE
BLACK AND WHITE PHOTOGRAPH

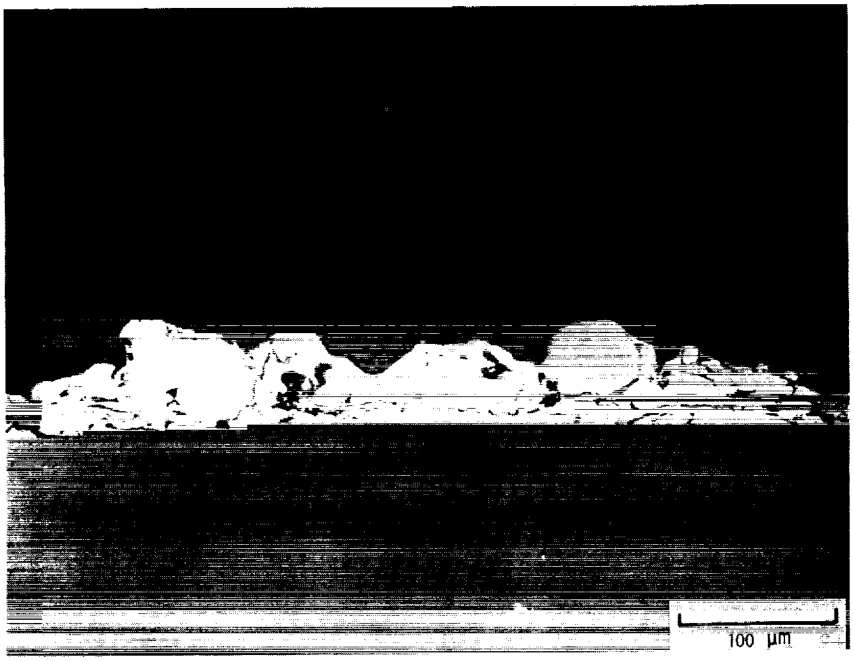

(a) TN1.

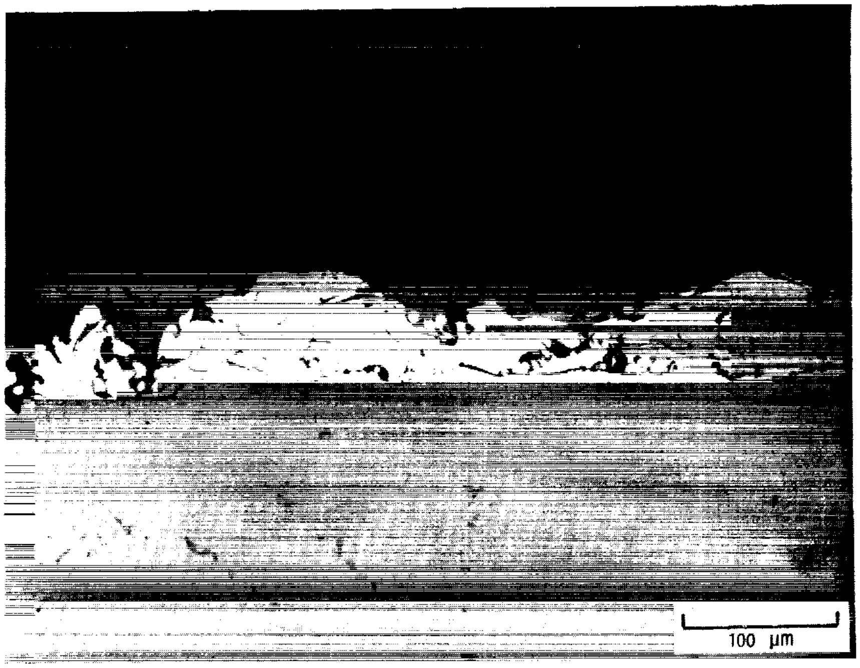

(b) TN2.

FIGURE 4. - CROSS-SECTIONAL MICROSTRUCTURES OF THE NASA-LeRC APPLIED ZrO_2-Y_2O_3 TBC'S.

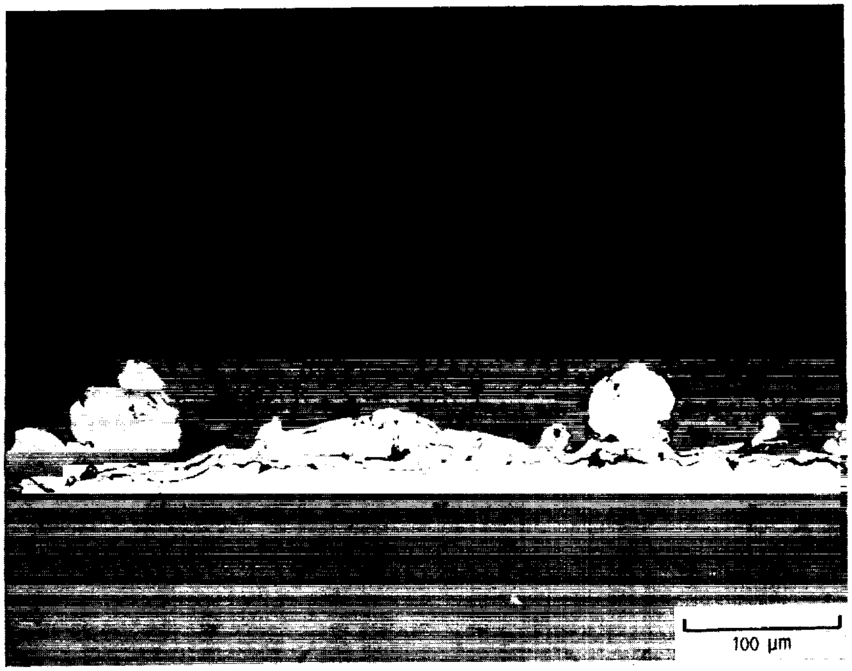

(c) TK1.

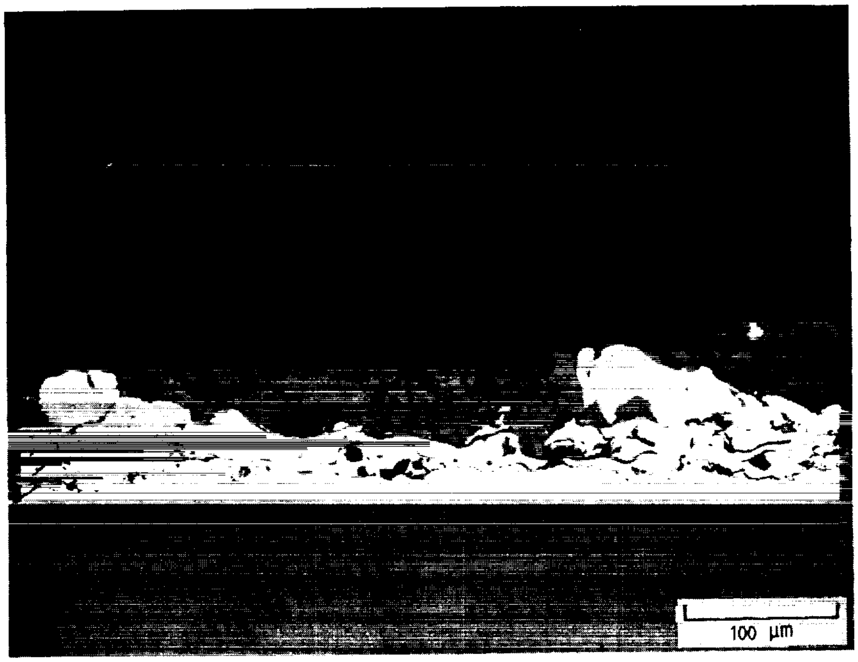

(d) TK2.

FIGURE 4. - CONCLUDED.

ORIGINAL PAGE
BLACK AND WHITE PHOTOGRAPH

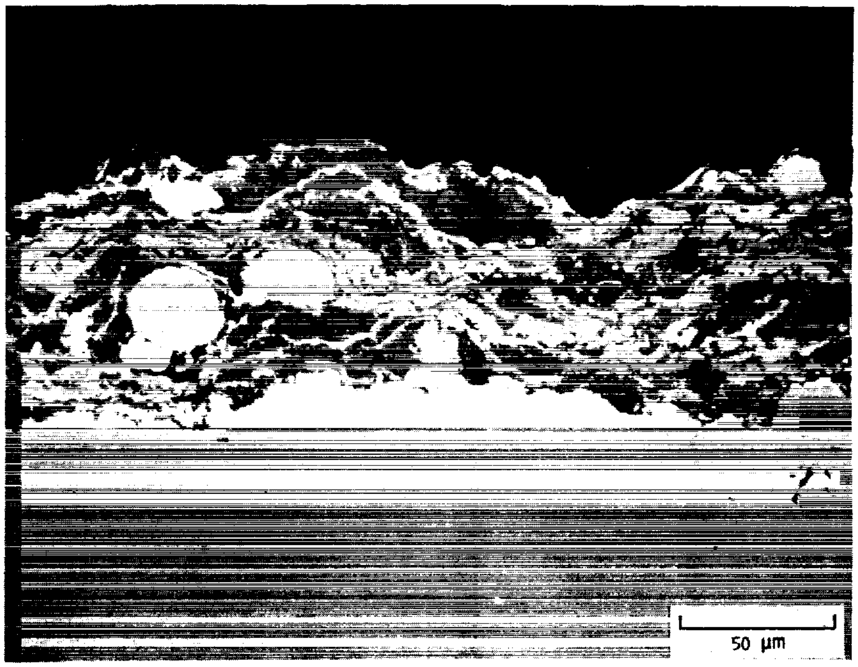

(a) LPPS 50/50CM.

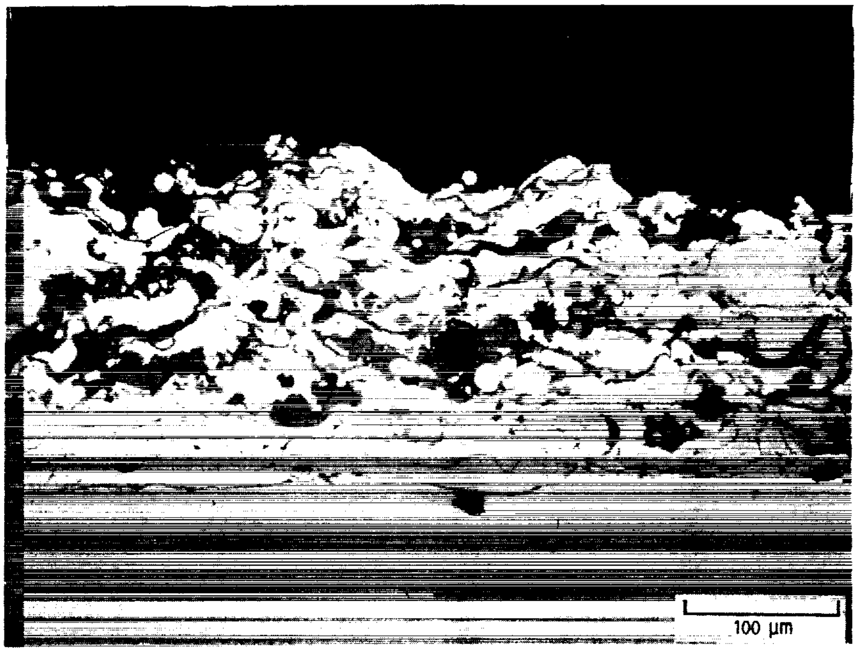

(b) APS 30/70CM.

FIGURE 5. - CROSS-SECTIONAL MICROSTRUCTURES OF THE CERMET TBC'S.

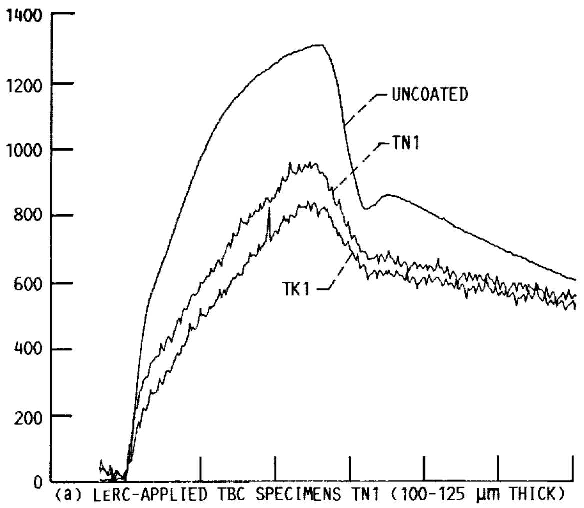

(a) LERC-APPLIED TBC SPECIMENS TN1 (100-125 μm THICK) AND TK1 (200-225 μm THICK). TEMPERATURES WERE MEASURED 0.0381-CM (0.015 IN.) BELOW THE TUBE SURFACE.

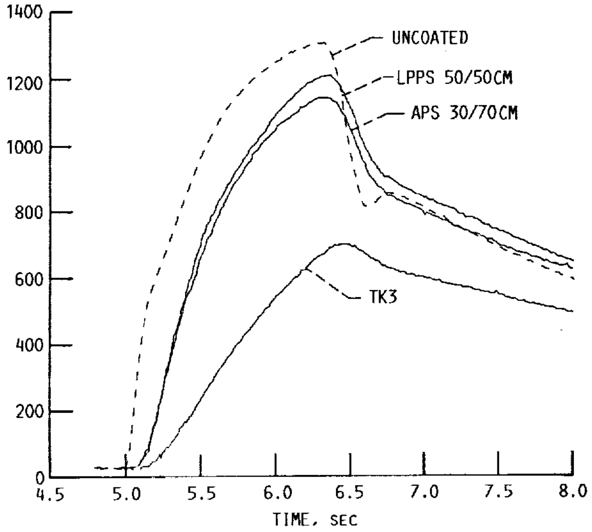

(b) SPECIMENS LPPS 50/50CM (50-70 μm THICK), APS 30/70CM (150-200 μm THICK). TEMPERATURES WERE MEASURED ON THE INNER WALL OF THE TUBE.

FIGURE 6. - TEMPERATURE PROFILES FOR VARIOUS TBC's. TEMPERATURES WERE MEASURED ON THE INNER WALL OF THE TUBE. NEAR-SURFACE TEMPERATURES (0.0381 CM BELOW SURFACE) MEASURED ON AN UNCOATED MAR-M246+Hf TUBE (REF. 3) ARE SHOWN FOR COMPARISON.

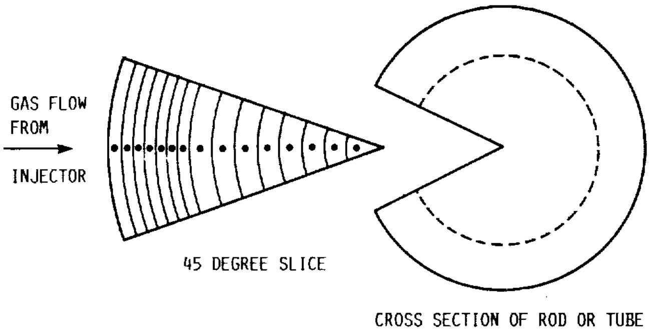

(a) 1-D MODEL OF THE ROD AND TUBE FOR HEAT TRANSFER TO THE STAGNATION POINT AND RADIAL HEAT TRANSFER.

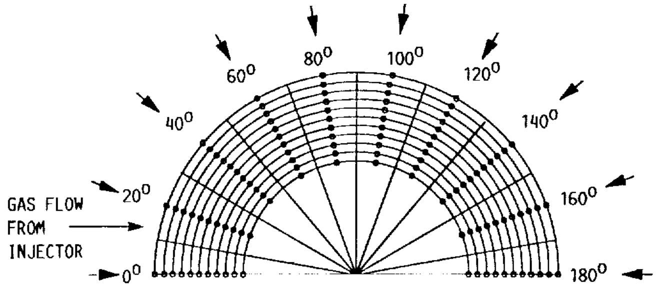

(b) 2-D MODEL OF A TUBE INCORPORATING RADIAL AND TANGENTIAL HEAT TRANSFER. ARROWS INDICATE POINTS OF COVECTIVE HEAT TRANSFER.

FIGURE 7. - SCHEMATIC VIEW OF THE THERMAL MODELS.

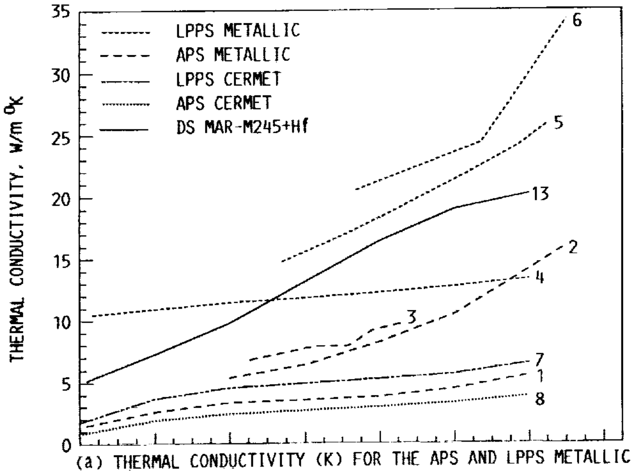

(a) THERMAL CONDUCTIVITY (K) FOR THE APS AND LPPS METALLIC COATINGS, AND THE DS MAR-M246+Hf SUBSTRATE.

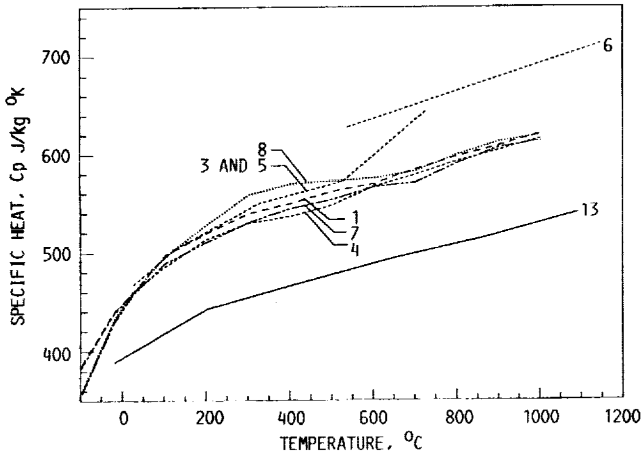

(b) SPECIFIC HEAT (Cp) FOR THE APS AND LPPS METALLIC COATINGS, THE CERMET COATINGS, AND THE DS MAR-M246+Hf SUBSTRATE.

FIGURE 8. - TEMPERATURE DEPENDENCE. COATING DESIGNATIONS AND REFERENCES ARE GIVEN IN TABLE IV.

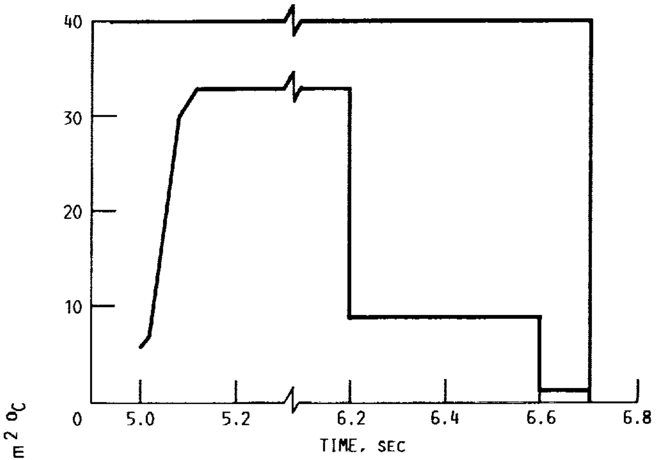

(a) TIME DEPENDENCE AT STAGNATION POINT (θ = 0°).

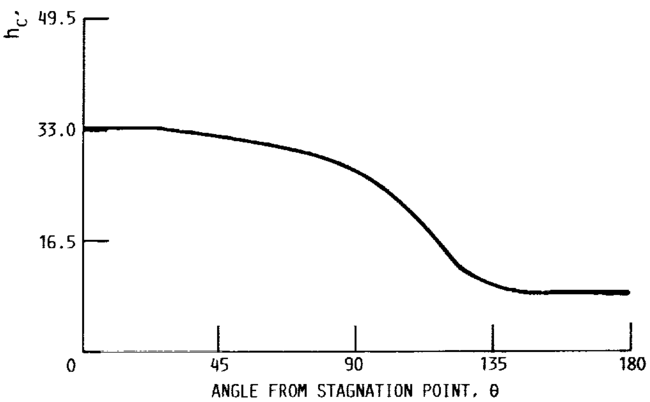

(b) ANGULAR DEPENDENCE AROUND 0.9525 CM (0.375 IN.) TUBE (REF. 3).

FIGURE 9. - HEAT TRANSFER COEFFICIENT.

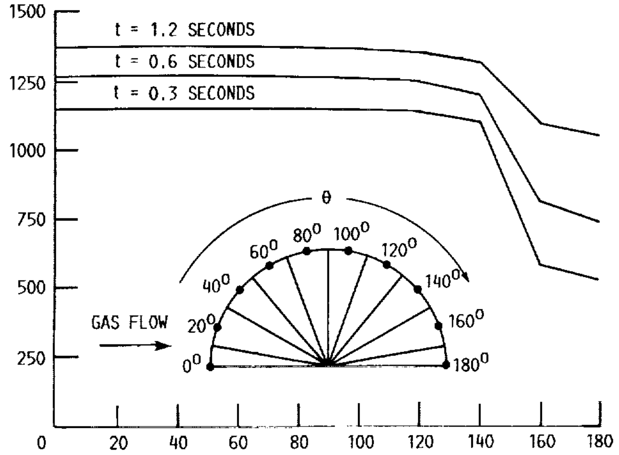

(a) ANGULAR TEMPERATURE DISTRIBUTION ON THE SURFACE OF THE TUBE AT VARIOUS TIMES WITH TANGENTIAL HEAT FLOW.

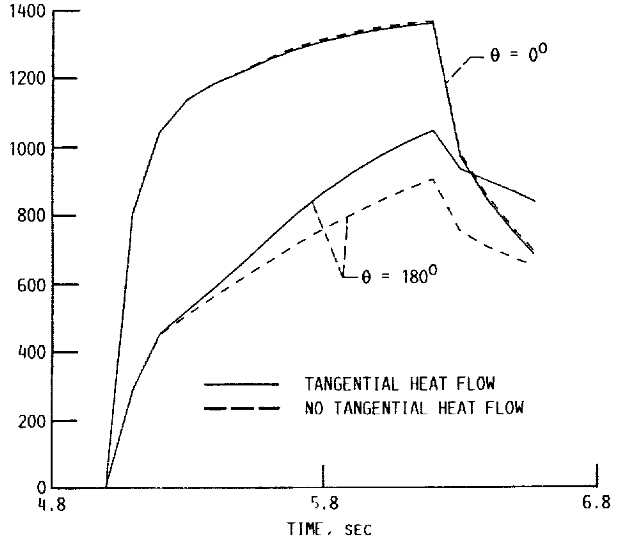

(b) TIME DEPENDENCE OF THE SURFACE TEMPERATURE AT θ = 0 (STAGNATION POINT) AND AT θ = 180°, (EXHAUST SIDE OF THE TUBE), WITH AND WITHOUT TANGENTIAL HEAT FLOW.

FIGURE 10. - PREDICTED TEMPERATURE PROFILES FOR AN UNCOATED TUBE USING THE 2-D MODEL.

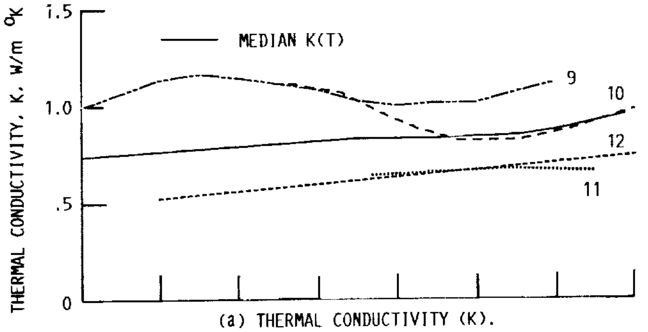

(a) THERMAL CONDUCTIVITY (K).

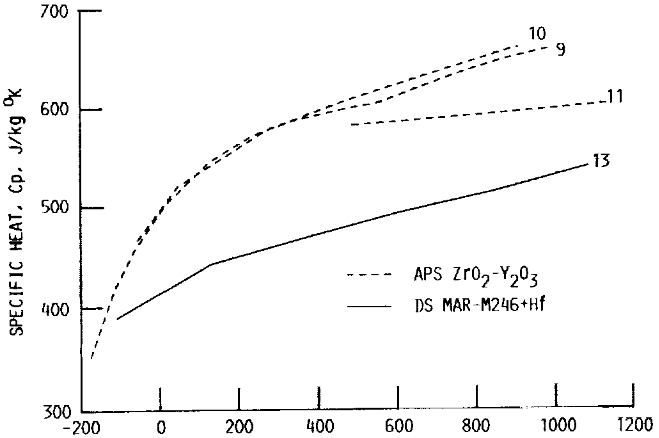

(b) SPECIFIC HEAT (Cp).

FIGURE 11. - TEMPERATURE DEPENDENCE FOR THE ZrO_2-Y_2O_3 CERAMIC COATINGS.

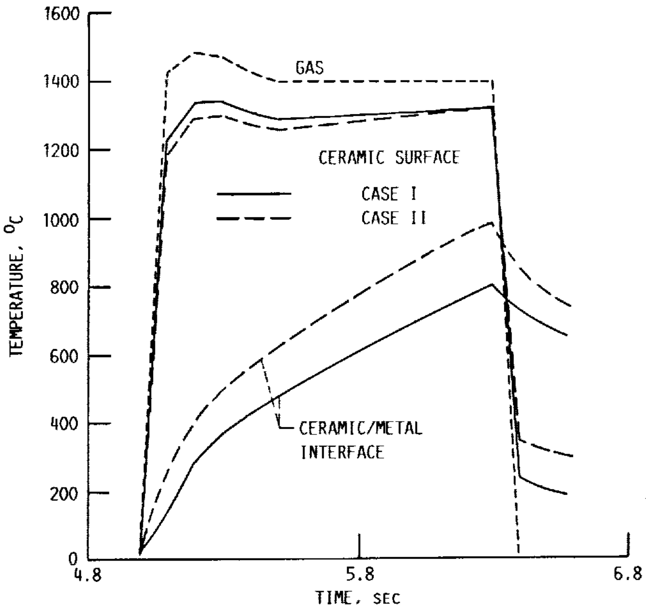

FIGURE 12. - PREDICTED TEMPERATURE PROFILES SHOWING THE EFFECT OF THE RANGE IN THE VALUES OF THE THERMAL CONDUCTIVITY FOR THE ZrO_2-Y_2O_3 CERAMIC COATING (SEE TEXT FOR A DESCRIPTION OF THE PARAMETERS USED IN EACH CASE).

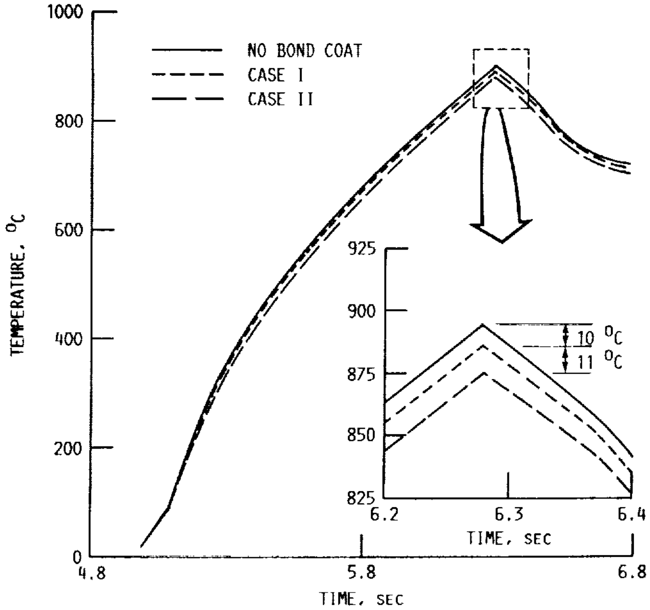

FIGURE 13. - PREDICTED TEMPERATURE PROFILES SHOWING THE EFFECT OF A 100 μm (0.004 IN.) METALLIC BOND COAT BELOW THE ZrO_2-Y_2O_3 CERAMIC TOP COAT. PREDICTED TEMPERATURES ARE FOR A LOCATION 0.038 CM (0.015 IN.) BELOW THE SUBSTRATE SURFACE OR BELOW THE BOND COAT/SUBSTRATE INTERFACE (SEE TEXT FOR A DESCRIPTION OF THE PARAMETERS USED IN EACH CASE).

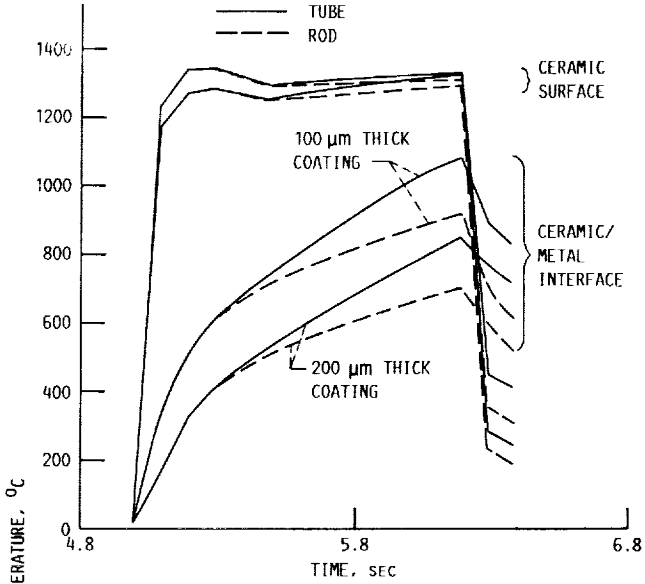

(a) TEMPERATURE VERSUS TIME FOR THE CERAMIC SURFACE AND AT THE CERAMIC/METAL INTERFACE.

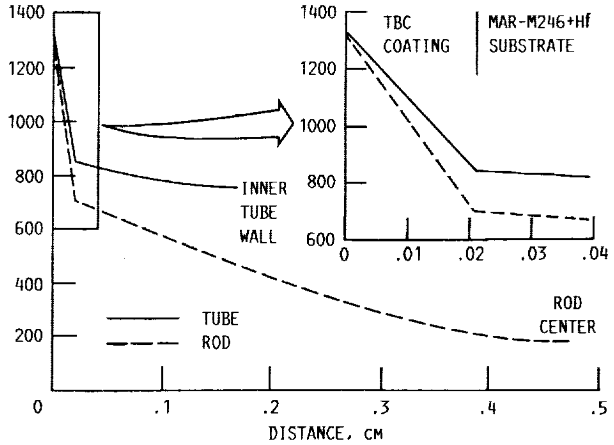

(b) RADIAL TEMPERATURE PROFILES FOR THE 200 μm (0.008 IN.) THICK TBC'S.

FIGURE 14. - PREDICTED TEMPERATURE PROFILES FOR A 100 AND 200 μm (0.004 AND 0.008 IN.) ZrO_2-Y_2O_3 TBC ON A TUBE AND ROD SUBSTRATE.

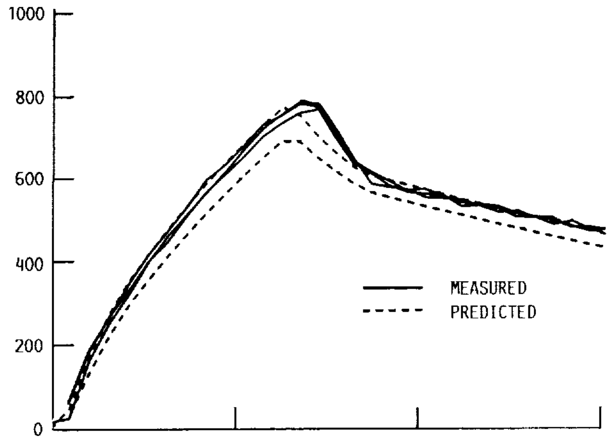

(a) NEAR-SURFACE TEMPERATURES FOR TK1 AND TK2.

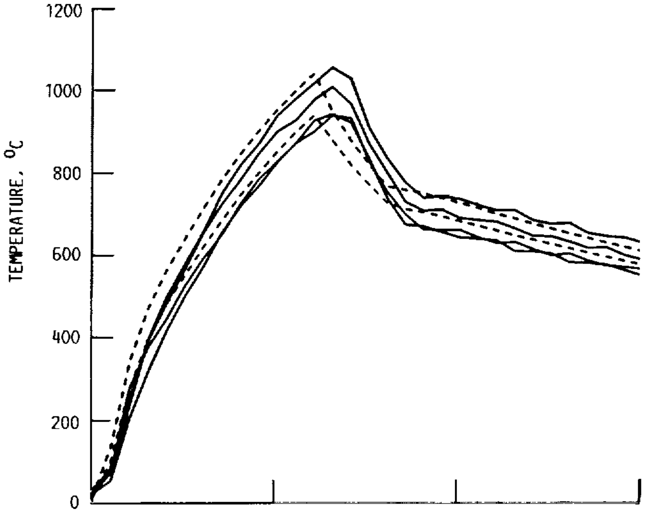

(b) NEAR-SURFACE TEMPERATURES FOR TN1 AND TN2.

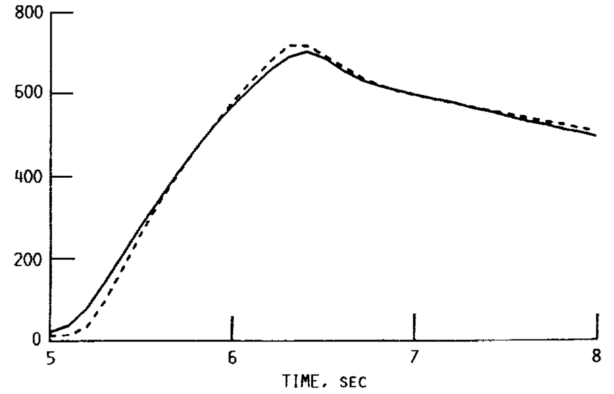

(c) INNER WALL TEMPERATURES FOR TK3.

FIGURE 15. - MEASURED AND PREDICTED TEMPERATURES FOR THE LERC-APPLIED ZrO_2-Y_2O_3 TBC's.

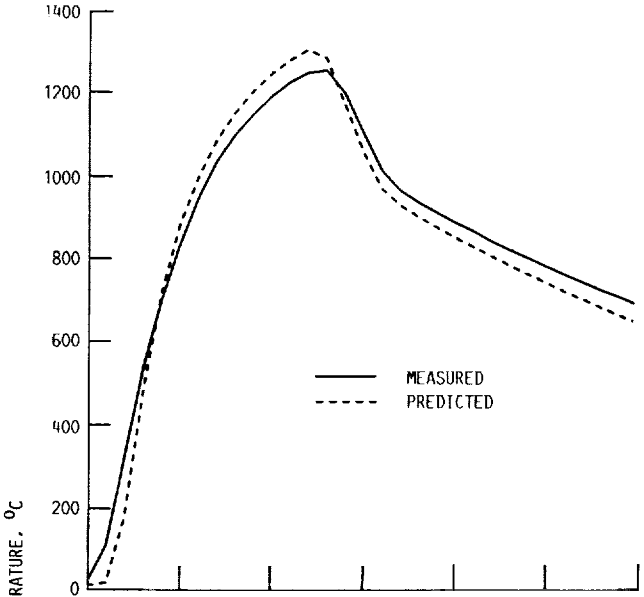

(a) LPPS 50/50CM

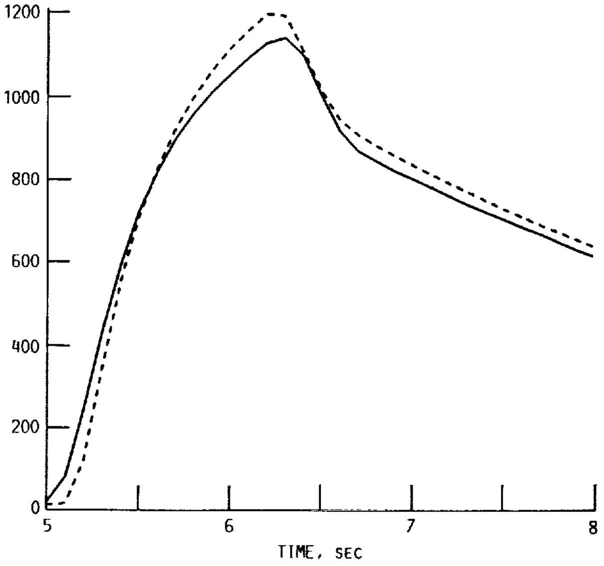

(b) APS 30/70CM

FIGURE 16. - MEASURED AND PREDICTED INNER WALL TEMPERATURES FOR THE CERMET COATED TUBES.

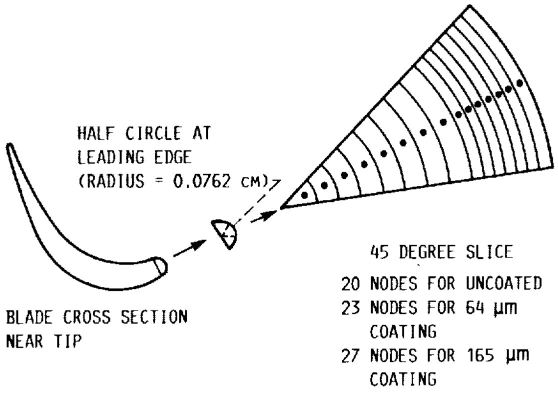

FIGURE 17. - SCHEMATIC VIEW OF THE THERMAL MODEL FOR THE LEADING EDGE OF THE HPFTP BLADE.

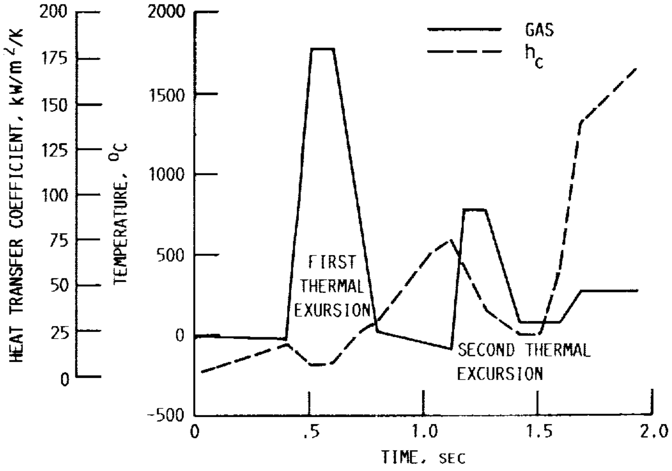

FIGURE 18. - TIME DEPENDENCE OF THE GAS TEMPERATURE IN THE HPFTP AND STAGNATION POINT HEAT TRANSFER COEFFICIENT FOR THE LEADING EDGE OF AN HPFTP BLADE DURING SSME START-UP.

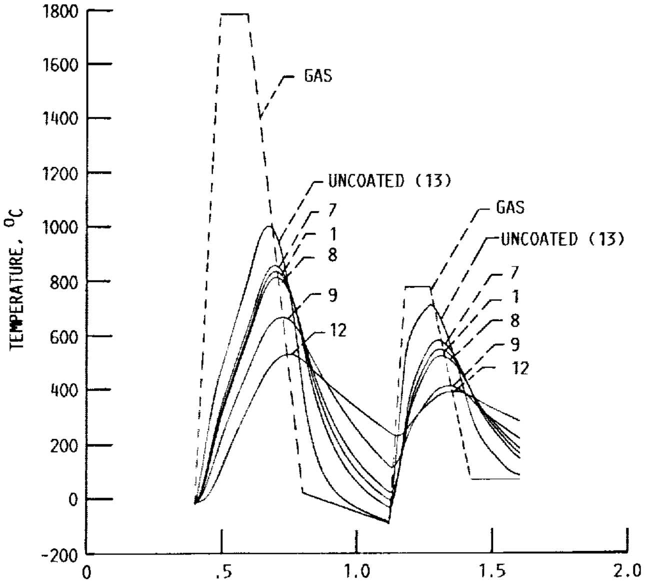

FIGURE 19. - PREDICTED METAL SURFACE TEMPERATURES DURING SSME START-UP FOR THE LEADING EDGE OF AN HPFTP BLADE WITH AND WITHOUT VARIOUS 165 μm (0.0065 IN.) THICK THERMAL BARRIER COATINGS.

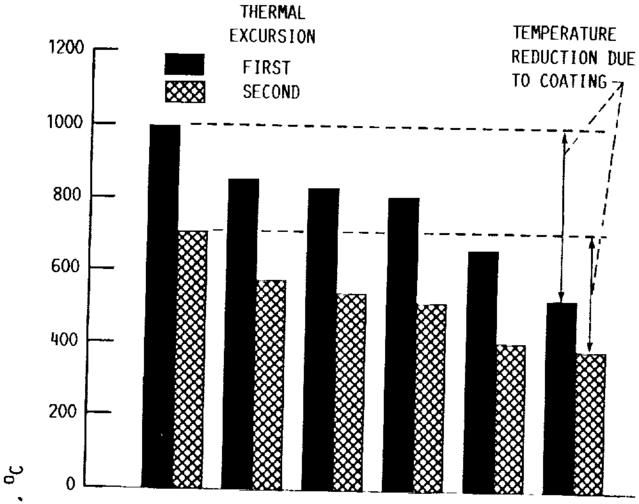

(a) WITH AND WITHOUT 165 μm (0.0065 IN.) THICK TBC's.

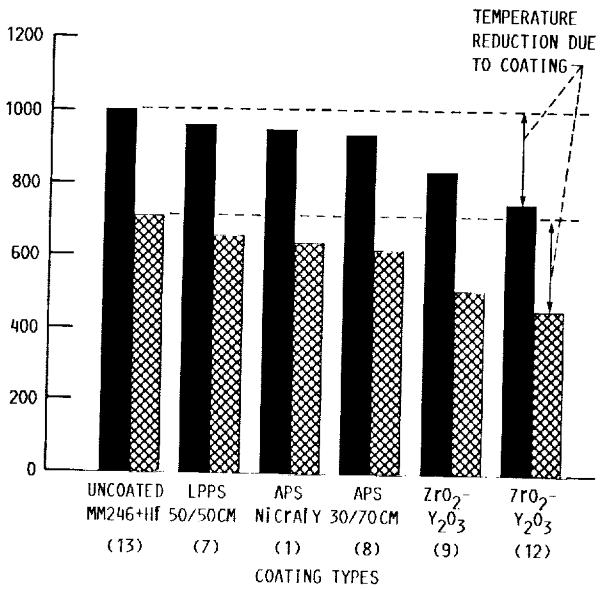

(b) WITH AND WITHOUT 64 μm (0.0025 IN.) THICK TBC's.

FIGURE 20. - MAXIMUM LEADING EDGE METAL TEMPERATURES FOR THE TWO THERMAL EXCURSIONS WHICH OCCUR DURING SSME START-UP.

National Aeronautics and
Space Administration

Report Documentation Page

1. Report No. NASA TM-102418	2. Government Accession No.	3. Recipient's Catalog No.

4. Title and Subtitle
Thermal Modelling of Various Thermal Barrier Coatings in a High Heat Flux Rocket Engine

5. Report Date
December 1989

6. Performing Organization Code

7. Author(s)
James A. Nesbitt

8. Performing Organization Report No.
E-5184

10. Work Unit No.
505-63-1A

9. Performing Organization Name and Address
National Aeronautics and Space Administration
Lewis Research Center
Cleveland, Ohio 44135-3191

11. Contract or Grant No.

13. Type of Report and Period Covered
Technical Memorandum

12. Sponsoring Agency Name and Address
National Aeronautics and Space Administration
Washington, D.C. 20546-0001

14. Sponsoring Agency Code

15. Supplementary Notes

16. Abstract

Traditional APS ZrO_2-Y_2O_3 TBC's and APS and LPPS ZrO_2-Y_2O_3/Ni-Cr-Al-Y cermet coatings were tested in a H_2/O_2 rocket engine located at the NASA Lewis Research Center. The traditional ZrO_2-Y_2O_3 thermal barrier coatings (TBC's) showed considerable metal temperature reductions during testing in the hydrogen-rich environment. A thermal model was developed to predict the thermal response of the tubes with the various coatings. Good agreement was observed between predicted temperatures and measured temperatures at the inner wall of the tube and in the metal near the coating/metal interface. The thermal model was also used to examine the effect of the differences in the reported values of the thermal conductivity of plasma sprayed ZrO_2-Y_2O_3 ceramic coatings, the effect of a 100 μm (0.004 in.) thick metallic bond coat, the effect of tangential heat transfer around the tube, and the effect of radiation from the surface of the ceramic coating. It was shown that for the short duration testing in the rocket engine, the most important of these considerations was the effect of the uncertainty in the thermal conductivity of traditional APS ZrO_2-Y_2O_3 TBC's which can amount to significantly different temperatures (>100 °C) predicted in the tube. The thermal model was also used to predict the thermal response of a coated rod in order to quantify the difference in the metal temperatures between the two substrate geometries and to explain the previously-observed increased life of coatings on rods over that on tubes. A thermal model was also developed to predict heat transfer to the leading edge of HPFTP blades during start-up of the space shuttle main engines. The ability of various TBC's to reduce metal temperatures during the two thermal excursions occurring on start-up was predicted. Temperature reductions of 150 to 470 °C were predicted for 165 μm (0.0065 in.) coatings for the greater of the two thermal excursions.

17. Key Words (Suggested by Author(s)) Thermal modelling; Thermal barrier coatings; High heat flux; Rocket engine coatings; Cermet coatings; TBC's; Rocket engine testing	18. Distribution Statement Unclassified – Unlimited Subject Category 26

19. Security Classif. (of this report)	20. Security Classif. (of this page)	21. No of pages	22. Price*
Unclassified	Unclassified	30	A03

NASA FORM 1626 OCT 86

*For sale by the National Technical Information Service, Springfield, Virginia 22161